International Geology Review
Publication details, including instructions for authors and subscription information:
http://www.informaworld.com/smpp/title~content=t902953900

Geochemistry of hornblende gabbros from Sonidzuoqi, Inner Mongolia, North China: implications for magmatism during the final stage of suprasubduction-zone ophiolite formation

Xiaohui Zhang [a]; Simon A. Wilde [b]; Hongfu Zhang [a]; Yanjie Tang [a]; Mingguo Zhai [a]
[a] State Key Laboratory of Lithospheric Evolution, Institute of Geology and Geophysics, Chinese Academy of Sciences, Beijing 100029, China [b] Department of Applied Geology, Curtin University of Technology, Perth, WA6845, Australia

Online Publication Date: 01 April 2009

To cite this Article Zhang, Xiaohui, Wilde, Simon A., Zhang, Hongfu, Tang, Yanjie and Zhai, Mingguo(2009)'Geochemistry of hornblende gabbros from Sonidzuoqi, Inner Mongolia, North China: implications for magmatism during the final stage of suprasubduction-zone ophiolite formation',International Geology Review,51:4,345 — 373
To link to this Article: DOI: 10.1080/00206810802712103
URL: http://dx.doi.org/10.1080/00206810802712103

International Geology Review
Vol. 51, No. 4, April 2009, 345–373

Taylor & Francis
Taylor & Francis Group

Geochemistry of hornblende gabbros from Sonidzuoqi, Inner Mongolia, North China: implications for magmatism during the final stage of suprasubduction-zone ophiolite formation

Xiaohui Zhang[a], Simon A. Wilde[b], Hongfu Zhang[a], Yanjie Tang[a] and Mingguo Zhai[a]

[a]*State Key Laboratory of Lithospheric Evolution, Institute of Geology and Geophysics, Chinese Academy of Sciences, Beijing 100029, China;* [b]*Department of Applied Geology, Curtin University of Technology, Perth, WA6845, Australia*

(*Accepted 22 December 2008*)

Allochthonous hornblende-rich gabbroic rocks at Sonidzuoqi constitute important components of the early to middle Palaeozoic orogen, which forms the southeastern part of the Central Asian orogenic belt in Inner Mongolia. Limited hornblende K–Ar and SHRIMP U–Pb zircon ages document the Late Silurian to Early Devonian gabbroic emplacement. The rocks are tholeiitic and are characterized by moderate large-ion-lithophile-element (e.g. Th, U) abundances, high-field-strength-element (e.g. Nb, Ta, Zr, Ti) depletions, high Ti/V ratios, and MORB-like isotopic signatures [$(^{87}Sr/^{86}Sr)_i \approx 0.7030$ to 0.7042; $\varepsilon_{Nd}(t) \approx +4.35$ to +7.80, $(^{206}Pb/^{204}Pb)_i \approx 17.46$ to 17.61]. These features argue for a hydrous basaltic parental magma. We postulate that the melt formed through the coupling of MORB-type mantle upwelling with aqueous fluid influx derived from slab devolatilization. This petrogenetic scenario suggests that an active spreading centre entered the trench during ridge subduction, bringing to a close an episode of suprasubduction-zone ophiolite formation. The Siluro-Devonian hornblende gabbros, together with a pre-490 Ma ophiolitic mélange of MORB-OIB affinity, ~483–471 Ma arc intrusions, ~498–461 Ma trondhjemite-tonalite-granodiorite plutons, and ~427–423 Ma calc-alkaline granites from the same area, provide documentation of multistage crustal generation processes during the life cycle of this suprasubduction-zone ophiolite.

Keywords: hornblende gabbro; geochemistry; petrogenesis; suprasubduction zone ophiolite; Central Asian Orogenic Belt

Introduction

Many suprasubduction zone (SSZ) ophiolites reflect a consistent sequence of events during their life cycles: birth = subduction initiation; youth = continued mantle wedge magmatism; maturity = stabilization during subduction; death = subduction of an active spreading ridge, and resurrection/accretionary uplift with obduction onto a continental margin (Shervais 2001; Shervais *et al.* 2004). This progression is generally evident through temporal and spatial geochemical changes that took place over the entire history of the oceanic basin (Shervais 2001; Shervais *et al.* 2004;

*Corresponding author. Email: zhangxh@mail.iggcas.ac.cn

ISSN 00200-6814 print/ISSN 1938-2839 online

DOI: 10.1080/00206810802712103
http://www.informaworld.com

Aldanmaz *et al.* 2008). Therefore, geochemical characterization of magmatic products from various stages of lithosphere production may shed light on the igneous processes and magma sources during the SSZ ophiolite life cycle, contributing to our understanding of the structure and magmatic evolution of oceanic crust formed at ancient spreading centres, and helping in interpreting the geological history of regions that comprise various accreted units in arc-basin systems (e.g. Pearce *et al.* 2003).

The Central Asian Orogenic Belt (CAOB) is a giant accretionary orogen that extends from the Urals to the Pacific, and from the Siberian and East European cratons to the North China and Tarim blocks (Figure 1(a) and (b); Sengör *et al.* 1993). It consists mainly of island arcs, ophiolites, oceanic islands, seamounts, accretionary wedges, oceanic plateaus and microcontinents comparable to that of Circumpacific Mesozoic-Cenozoic accretionary orogens (Khain *et al.* 2002, 2003; Xiao *et al.* 2003; Windley *et al.* 2007). Its protracted history is recorded by constituent ophiolites, mostly of SSZ type, which were generated episodically in the late Mesoproterozoic (Khain *et al.* 2002), the Neoproterozoic (Kuzmichev *et al.* 2005), the early Palaeozoic (Jian *et al.* 2008) and the late Palaeozoic (Xiao *et al.* 2003; Miao *et al.* 2007).

The southeastern part of the CAOB – the Manchurides of Sengör and Natal'in (1996) or the Xing-Meng orogenic belt (Wu *et al.* 2002) – lies immediately north of the North China craton, and is separated from the Altaid accreted terranes (Sengör and Natal'in 1996) by the intervening Palaeo-Asian ocean. Its most prominent tectonic feature is the association of paired orogens: the southern orogen is typified by an arc-trench complex and the northern orogen by a ridge-trench complex (Jian *et al.* 2008). The paired orogens exhibit a consistent progression from ocean-floor subduction/arc formation, ridge subduction, to microcontinent accretion/collision, as recorded by the successive phases of a SSZ ophiolite sequence. The geological

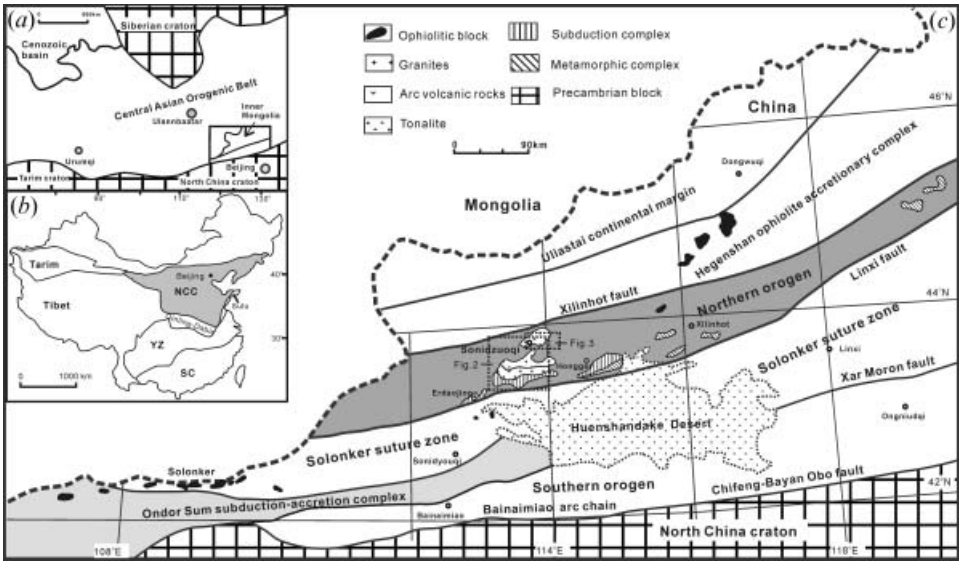

Figure 1. (a) Tectonic setting of the Mongolian segment of the Central Asian Orogenic Belt. (b) Major tectonic divisions of China, where NCC, YZ and SC denote the North China craton, Yangtze craton and South China orogen, respectively. (c) Geological sketch map of Inner Mongolia showing the Solonker suture zone separating the northern and southern orogens (modified after Jian *et al.* 2008).

characteristics of these ophiolitic fragments reflected the evolution of the early to middle Palaeozoic terranes of Inner Mongolia and are central to our understanding of the Palaeozoic continental growth of the long-lived CAOB. However, no substantial magmatism associated with the death of the SSZ ophiolite has been documented thus far.

In this contribution, we present new geochemical and Sr–Nd–Pb isotopic data on the mafic intrusive rocks at Sonidzuoqi, with the aim of examining their petrogenetic features in order to establish their tectono-magmatic significance within the life cycle of a SSZ ophiolite. This may provide new constraints on the evolution of arc-basin systems in the CAOB.

Geological setting

As documented by Jian *et al*. (2008), the presence of paired orogens is the striking tectonic feature in Inner Mongolia (Figure 1(c)). They were separated by the Solonker suture zone, which extends from Solonker, via Sonidyouqi, to Xilinhot and then further west and northeast into Jilin province where it has been variously named as the Sunluo suture (Davis *et al.* 2001), the Tian Shan-Ying Shan suture (Yin and Nie 1996), the Hegenshan-Neijiang-Heihe suture (Wu *et al.* 2002), and the Solon Obo-Linxi suture (Liu *et al.* 2005). This suture records the terminal evolution of the CAOB in Inner Mongolia (Xiao *et al.* 2003).

The southern orogen is located to the south of the Solonker suture and mainly consists of a subduction complex, an ophiolite belt and an island arc chain (Jian *et al.* 2008). The first two constitute the Ondor Sum subduction-accretion complex that comprises turbidites, olistostrome mélanges and blueschists (Hu *et al.* 1990; Xiao *et al.* 2003). The ophiolite mélange forms an elongate, nearly E-W trending belt (Hu *et al.* 1990; Wang *et al.* 1991) and documents successive magmatism during its life cycle (Jian *et al.* 2008): the 497–477 Ma Tulinkai ophiolite during its birth; the 473–470 Ma mantle wedge magmatism during its youth; the 461–450 Ma adakitic magmatism during its maturity (Liu *et al.* 2003); the 451–434 Ma high-grade metamorphism indicative of subduction of a ridge crest; and the 428–423 Ma boninitic magmatism suggesting ridge collision with the ophiolite (Jian *et al.* 2008). To the south of the ophiolite belt, the Bainaimiao arc chain is in fault contact with the North China craton. This magmatic arc exhibits three major coherent phases: 488–444 Ma arc volcanism (Tao *et al.* 2005); 448–438 Ma adakitic plutonism (Jian *et al.* 2008); and 419–415 Ma magmatism related to collision of the arc with a passive continental margin (Shong *et al.* 2003).

At Sonidzuoqi, the northern orogen (Figure 1(c)) forms a north-dipping thrust belt (Xiao *et al.* 2003). This distinct tectonic zone includes the following units from south to north: (1) a metamorphic complex (Tang 1990; Shi *et al.* 2003); (2) an ophiolitic mélange and associated sedimentary cover (Xu and Chen 1997); (3) an extensive plutonic unit with arc affinity (Shi *et al.* 2005a); (4) a trondhjemite-tonalite-granodiorite (TTG) plutonic unit (Chen *et al.* 2000; Jian *et al.* 2008); and (5) collision-related granitic magmatic rocks (Shi *et al.* 2005b).

The discontinuous metamorphic unit, generally designated as the Xilinhot complex (Tang 1990), mainly consists of paragneiss, orthogneiss, schist, quartzite, amphibolite and ultramafic rocks. The typical mineral assemblage of the paragneiss includes kyanite, staurolite and garnet, indicating medium-pressure metamorphism (Shi *et al.* 2003; Zhu *et al.* 2004). The rocks were interpreted as predominantly forearc sediments with a minor oceanic crustal component (Shi *et al.* 2003). SHRIMP U–Pb dating of a

gneiss sample yielded a magmatic zircon age of ca. 437 Ma, with additional inherited zircon ages of ca. 600–900 Ma and 1850–3100 Ma (Shi *et al.* 2003).

The ophiolitic mélange mainly crops out from Erdaojing to Hongger (Figures 1 and 2) and comprises variably sized blocks of serpentinized harzburgite, dunite, cumulate pyroxenite, pillow basalt, volcanoclastic rocks and chert, and blueschist (Wang *et al.* 1991; Xu and Chen 1997; Zhang and Wu 1999; Huang *et al.* 2006). Amphibole $^{40}Ar/^{39}Ar$ dating of blueschist gave an age of 383 ± 13 Ma (Xu *et al.* 2001). The mélange is unconformably overlain by a Late Devonian (ca. 360 Ma) conglomerate (the Serobao Formation) (Xu *et al.* 2001).

The plutonic arc rocks occur mainly at Shadui (Figure 2). They were intruded into basalt and chert of the Erdaojing ophiolitic complex and mainly consist of cumulate gabbro, quartz diorite, small anorthosite blocks, tonalite dikes, and small bodies of gneissic granite (Jian *et al.* 2008). SHRIMP U–Pb zircon dating of the cumulate gabbro, quartz diorite and tonalite yielded emplacement ages of 483 ± 2, 480 ± 2 and 471 ± 2 Ma, respectively (Jian *et al.* 2008).

The Baiyanbaolidao TTG plutonic unit also intruded into the Erdaojing complex. It is composed of variably deformed diorite, quartz diorite, tonalite and granodiorite (Chen *et al.* 2000; Shi *et al.* 2005a). SHRIMP U–Pb zircon dating of a diorite sample

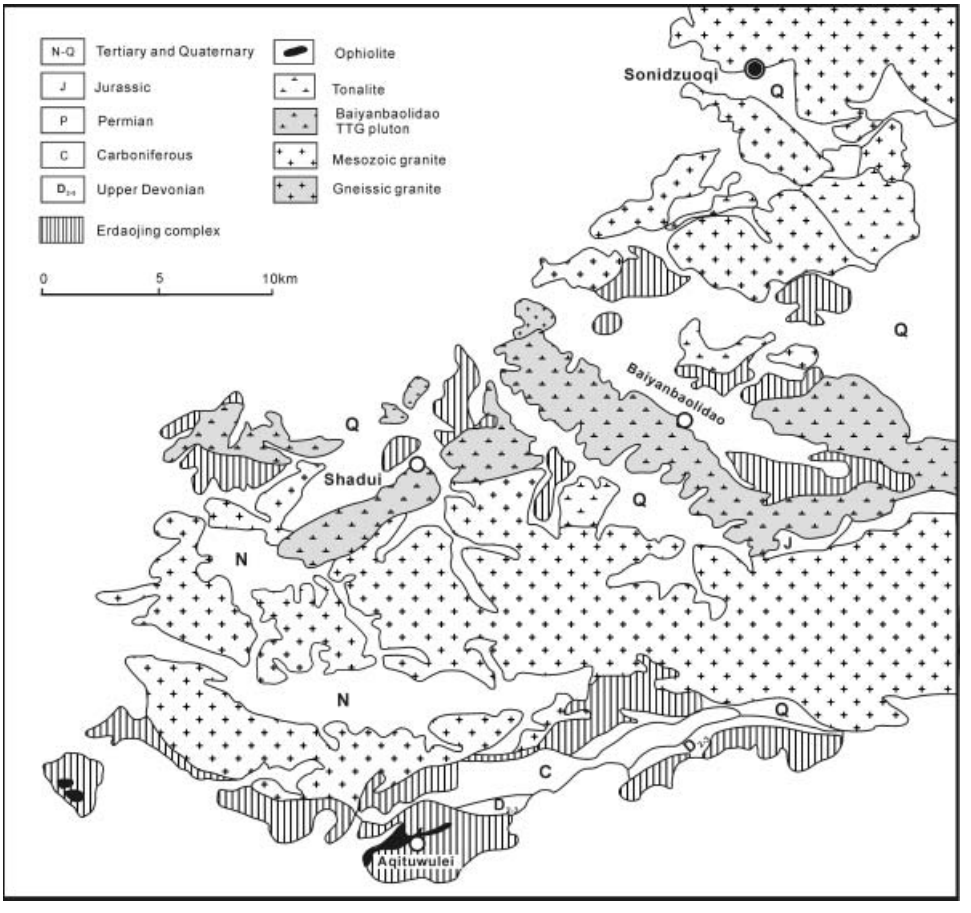

Figure 2. Geological map of the Sonidzuoqi area within the northern orogen (modified from Jian *et al.* 2008).

yielded a crystallization age of 490 ± 8 Ma, with inherited xenocryst ages ranging from 760 to 717 Ma (Chen *et al.* 2000), while magmatic zircons from tonalite samples gave emplacement ages from 481 to 464 Ma (Jian *et al.* 2008). In addition, two granite samples have ages of 427–423 Ma (Shi *et al.* 2005b).

Besides these relatively well-dated units, numerous allochthonous ophiolitic mafic-ultramafic bodies occur along the Solonker suture zone. They are chiefly characterized by hornblende gabbros and constitute the focus of this study.

The late Palaeozoic Solonker suture zone marks the site of final closure of the Palaeo-Asian ocean, and includes late Palaeozoic ophiolitic complexes at Solonker (Jian *et al.* 2008) and Hegenshan (Miao *et al.* 2007) (Figure 1(c)), Carboniferous magmatic arc rocks (Chen *et al.* 2000), Early Permian post-collisional bimodal volcanic rocks (Zhang *et al.* 2008) and Late Permian A-type granites (Shi *et al.* 2004). There is controversy regarding the time of its suturing. Some authors propose that it took place during the Permian to Early Triassic (Sengör *et al.* 1993; Chen *et al.* 2000; Xiao *et al.* 2003); whereas others suggest it occurred during either the Middle Devonian (Tang 1990) or Late Devonian to Early Carboniferous (Shao 1991; Hong *et al.* 1995); still others advocate a middle Mesozoic age (Nozaka and Liu 2002). However, our recent documentation of the Early Permian post-collisional bimodal volcanism in central Inner Mongolia suggest that the North China craton and Mongolian micro-continents amalgamated by the earliest Permian and this resulted in the Mesozoic North China-Mongolian Plate (Zhang *et al.* 2008).

Petrography

The Sonidzuoqi gabbroic rocks are widely exposed as isolated bodies within the late Palaeozoic magmatic arc belts (Figure 3). They are dark green gabbros that are medium- to coarse-grained with intergranular texture, and are in fault contact with the host magmatic rocks. Typical samples mainly consist of amphibole, pyroxene, plagioclase, with minor quartz and accessory ilmenite, zircon and apatite. Amphibole, the most abundant mafic mineral, mainly occurs as subhedral to euhedral phenocrysts and is locally altered to calcite and chlorite. All amphiboles belong to the sodic-calcic group ($Ca + Na \geq 1$ and $0.5 < Na < 1.5$) according to

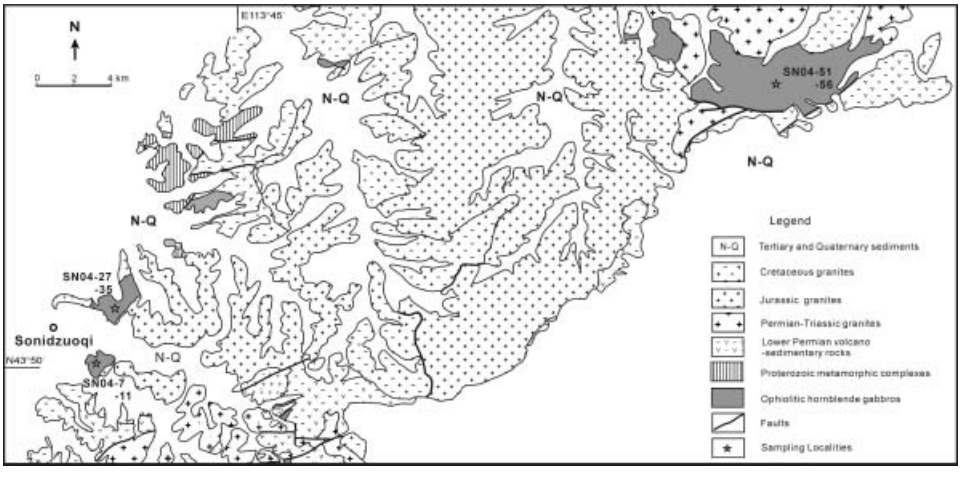

Figure 3. Detailed geological map of the Sonidzuoqi region showing the distribution of the hornblende gabbros, including sample sites (modified from IMBGMR 1998).

the classification of Leake *et al.* (1997) and can be classified as tschermakite, magnesio-hornblende and actinolite. Pyroxene mainly occurs as relicts in the centres of magnesio-hornblendes and is dominantly augite. Plagioclase also occurs as phenocrysts, which are generally subhedral laths with occasional combined albite and carlsbad–albite twinning and range in anorthite content from An_{92} to An_{53}. They are partly altered to sericite, calcite and epidote.

Analytical methods

We adopted both zircon U–Pb and hornblende K–Ar methods to constrain the emplacement age of the gabbros. Both minerals were separated from a fresh hornblende gabbro sample (SN04-8) using standard density and magnetic separation techniques and purified by hand-picking under a binocular microscope. Zircons were dated on a SHRIMP II ion microprobe at Curtin University of Technology. Data were processed using the SQUID (1.02) and ISOPLOT programs (Ludwig 2001). Corrections of Pb/U ratios were made by normalization to zircon standard CZ3 ($^{206}Pb/^{238}Pb=0.0914$, corresponding to an age of 564 Ma). The data were corrected for common lead using the measured ^{204}Pb. Uncertainties in individual analyses are reported at the 1σ level, whereas pooled ages are quoted at the 95% (2σ) level.

Hornblende K–Ar age determination was carried out on a MM5400 mass spectrometer at the Research Institute of Petroleum Exploration and Development, China National Petroleum Cooperation, following the procedure described by Fan *et al.* (2003).

For elemental and isotopic analyses, samples were grounded in an agate mill to ~200 mesh. Major oxides were analysed with a Phillips PW 2400 X-ray fluorescence spectrometer (XRF) at the Institute of Geology and Geophysics, Chinese Academy of Sciences (IGGCAS). Trace element abundances were obtained on a VG-PQII ICP-MS also at the IGGCAS. Samples were dissolved in distilled $HF + HNO_3$ in 15 ml high-pressure Teflon bombs at 120°C for six days, dried and then diluted to 50 ml for analysis. A blank solution was prepared and the total procedural blank was <50 ng for all trace elements. Indium was used as an internal standard to correct for matrix effects and instrument drift. Precision for all trace elements is estimated to be 5% and accuracy is better than 5% for most elements based on analyses of the GSR-3 standard (see Zhang *et al.* 2008).

Sr, Nd and Pb isotopic compositions were measured on a Finnigan Mat 262 thermal ionization mass spectrometer at the IGGCAS. For Sr and Nd determination, the powders were washed with 0.3 N HCL for 1 h at ca. 100°C, and dried after rinsing with purified water. The samples were weighed and spiked with mixed isotope tracers, dissolved in Teflon capsules with $HF + HNO_3$ at 120°C for seven days, and separated by standard cation-exchange techniques. Procedural blanks were <100 pg for Sm and Nd and <500 pg for Rb and Sr. $^{143}Nd/^{144}Nd$ was corrected for mass fractionation by normalization to $^{146}Nd/^{144}Nd=0.7219$, and $^{87}Sr/^{86}Sr$ ratios normalized to $^{86}Sr/^{88}Sr=0.1194$. Typical within-run precision (2σ) for Sr and Nd was estimated to be 0.00002 and 0.000015, respectively. The measured values for the La Jolla Nd standard and NBS-607 Sr standard were $^{143}Nd/^{144}Nd=0.511853$ and $^{87}Sr/^{86}Sr=1.20042$ during the period of data acquisition. For Pb isotope determination, the powders were dissolved in Teflon vials with purified HF at 120°C for six days and then separated using anion-exchange columns (AG1 × 8, 200–400 resin) with diluted HBr as elutant. Repeat analyses of NBS981 yielded $^{206}Pb/^{204}Pb=16.917\pm0.008$, $^{207}Pb/^{204}Pb=15.460\pm0.010$, $^{208}Pb/^{204}Pb=$

36.617 ± 0.011. The Pb data were corrected based on the NBS981 recommended data. Precision of lead isotope ratios is within ± 1‰.

Analytical results

Geochronology

Due to the generally small size and rarity of the zircons, we only managed to date three zircons. They show scatter with $^{206}Pb/^{238}U$ ages of 394 ± 5, 374 ± 5 and 429 ± 7 Ma (Table 1; Figure 4). Meanwhile, the hornblende K–Ar dating yielded an apparent age of 417 ± 3 Ma (Table 2). The relatively good agreement shown by two dating results suggests that the hornblende gabbros at Sonidzuoqi were emplaced during the Late Silurian to Early Devonian times.

Major oxides and trace elements

Major and trace element analyses are presented in Table 3. The rocks have moderate SiO_2 (47.16–50.03 wt-%), TiO_2 (1.36–2.95 wt-%) and Al_2O_3 (15.16–16.15 wt-%), high TFe_2O_3, MgO (5.03–9.02 wt-%), CaO (9.90–11.23 wt-%) and transitional metal elements, low contents of alkalis and P_2O_5 (0.01–0.39 wt-%). On the SiO_2 vs Zr/TiO_2 diagram of Winchester and Floyd (1977) (Figure 5(a)), the gabbros exclusively plot in the field of sub-alkaline basalt. They also exhibit a low-K tholeiitic character (Figure 5(b) and (c)).

The gabbros are characterized by moderate concentrations of total REEs ($\sum$REE = 43.8 to 65.1 ppm), flat to slightly depleted LREE-enriched patterns (La_N/Yb_N = 0.89 to 1.54) with weak Eu anomalies (Eu/Eu^* = 0.81 to 1.14; Figure 6(a); Table 3). In the primitive mantle-normalized spidergram (Figure 6(b)), they show moderate enrichment in LILE (e.g. Th, U), depletion in HFSE (Nb, Ta, Zr, Hf), variable concentrations of Rb and K and a strong positive Pb anomaly.

Sr–Nd–Pb isotopic compositions

The results of Sr–Nd isotope analyses are presented in Table 4. The initial isotopic ratios were calculated based on the age of 420 Ma. As shown in a plot of $\varepsilon_{Nd}(t)$ vs $(^{87}Sr/^{86}Sr)_i$ (Figure 7), the rocks exhibit a fairly restricted range of isotopic compositions with initial $^{87}Sr/^{86}Sr$ ratios of 0.7030 to 0.7042, strongly positive $\varepsilon_{Nd}(t)$ values of +4.35 to +7.80 and model ages (T_{DM2}) of 504 to 783 Ma. Most plot in the MORB field.

The gabbros also have prominent positive Δ8/4 (81.1 to 108.7) and moderately high Δ7/4 (11.26–15.95) values with $(^{206}Pb/^{204}Pb)_I$ = 17.46 to 17.61, $(^{207}Pb/^{204}Pb)_i$ = 15.50 to 15.55, and $(^{208}Pb/^{204}Pb)_i$ = 37.74 to 37.91 (Table 5). In the $(^{207}Pb/^{204}Pb)_i$ and $(^{208}Pb/^{204}Pb)_i$ vs $(^{206}Pb/^{204}Pb)_i$ correlation plots (Figure 8(a) and (b)), they fall well above the Northern Hemisphere Reference Line (NHRL) and lie within or close to the I-MORB field.

Discussion

Petrogenesis

Hydrous petrographic character

Petrographically, the Sonidzuoqi gabbros are remarkably similar to the high-level homogeneous hornblende gabbros from Central Anatolia in Turkey (Kocak *et al.*

Table 1. SHRIMP U–Pb zircon data for Sonidzuoqi hornblende gabbro sample SN04-8.

Spot	U (ppm)	Th (ppm)	Th/U	Pb (ppm)	$f_{206\ (\%)}$	$^{207}Pb/^{206}Pb$ ($\pm$%error 1σ)	$^{206}Pb/^{238}U$ ($\pm$%error 1σ)	$^{207}Pb/^{235}U$ ($\pm$%error 1σ)	Age (Ma) $^{206}Pb/^{238}U \pm 1\sigma$	Age (Ma) $^{207}Pb/^{206}Pb \pm 1\sigma$
SN8-2	350	535	1.58	18	0.46	0.0546 $\pm$ 3	0.0598 $\pm$ 1	0.45 $\pm$ 4	374 $\pm$ 5	374 $\pm$ 5
SN8-3	241	61	0.26	14	0.57	0.0538 $\pm$ 4	0.0687 $\pm$ 2	0.51 $\pm$ 4	427 $\pm$ 6	429 $\pm$ 7
SN8-4	716	313	0.45	39	0.92	0.0523 $\pm$ 6	0.0629 $\pm$ 1	0.45 $\pm$ 5	393 $\pm$ 5	394 $\pm$ 5

Note: f_{206} = percentage of common ^{206}Pb in the total measured ^{206}Pb.

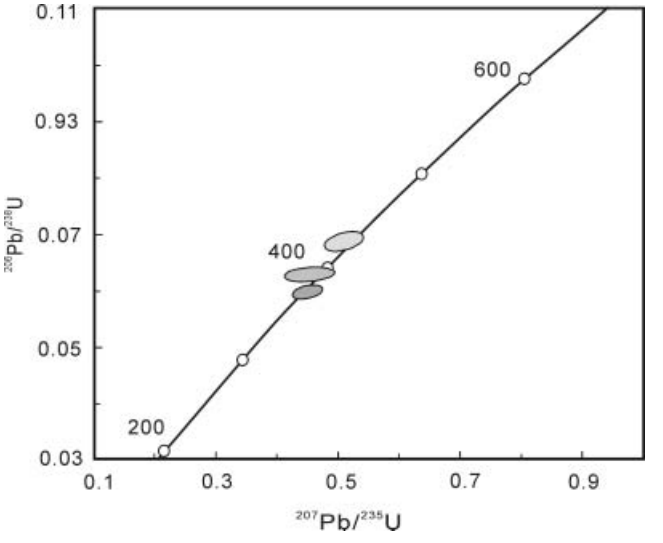

Figure 4. U–Pb zircon concordia diagram for sample SN04-8 from the Sonidzuoqi hornblende gabbros.

2005), including the development of three different types of hornblendes and the dominance of calcic plagioclase.

Such distinctive petrographic features are broadly typical of mafic-ultramafic intrusions within island arc settings. First, the occurrence of different hornblendes seems consistent with high P_{H2O} conditions in the magma. Specifically, tschermakite appears to have directly crystallized in the very wet magma after crystallization of olivine, pyroxene and calcic plagioclase, while the magnesio-hornblendes might have been formed as secondary amphiboles by reaction of the earlier pyroxene with the increasingly water-rich magma. Second, as experimentally confirmed by Johannes (1978), high water-pressure can cause plagioclase compositions to be anorthite-rich in the albite-anorthite-water system. Arculus and Wills (1980) also noted that hydrous basaltic melts crystallize more anorthitic plagioclase than anhydrous melts. Moreover, Burns (1985) argued that gabbroic rocks occurring within an arc-like environment differ from their oceanic equivalents in terms of the high Ca-content in plagioclase. Therefore, the dominance of calcic plagioclase in the Sonidzuoqi gabbros may indicate an island arc setting. Third, the Ca-rich composition of clinopyroxene also attests to a water-rich setting, since pyroxenes containing little Ca do not crystallize from wet basaltic or basaltic andesite melts (Sisson and Grove 1993).

Dual geochemical affinity

As evident from petrographic observation, the Sonidzuoqi hornblende gabbros have undergone variable degrees of chemical alteration, although it is unclear whether the alteration is from seafloor hydrothermal metamorphism, regional metamorphism or both. Metamorphism is sub-greenschist facies, and it has produced an assemblage of chlorite + actinolite + albite + quartz $\pm$ ilmenite. As documented by numerous studies on the effects of this kind of alteration on the geochemistry of ophiolitic rocks (e.g. Pearce and Norry 1979; Coish *et al.* 1982; Bedard 1999), this process may have changed the concentration of some geochemically mobile trace elements, especially

Table 2. Hornblende K–Ar data for Sonidzuoqi hornblende gabbro sample SN04-8.

Sample	Weight (g)	K (%)	^{40}Ar total ($\times 10^{-10}$ mol/g)	^{40}Ar radiogenic ($\times 10^{-10}$ mol/g)	^{40}K ($\times 10^{-9}$ mol/g)	^{40}Ar/^{40}K	Age ($\pm 1\sigma$) (Ma)
SN04-8	0.01264	0.17	2.0225	1.386	5.075	0.027311	417.7 ± 3.2

Note: Parameters for ^{40}K: $\lambda_e = 0.581 \times 10^{-10}$ year^{-1}; $\lambda_\beta = 4.962 \times 10^{-10}$ year^{-1}; ^{40}K = 0.01167 at.-% (Steiger and Jäger 1977).

Table 3. Major and trace element data for Sonidzuoqi hornblende gabbros.

Sample No.	SN04-5	SN04-7	SN04-9	SN04-11	SN04-27	SN04-29	SN04-34	SN04-51	SN04-52	SN04-54	SN04-56
SiO_2	49.46	49.37	49.27	50.03	49.06	49.01	48.54	48.75	47.97	49.09	47.16
TiO_2	1.45	1.4	1.78	1.78	1.36	1.46	1.21	1.49	1.02	2.09	2.95
Al_2O_3	15.16	15.61	15.16	15.26	15.52	15.62	16.28	16.15	16.21	15.25	14.68
Fe_2O_{3T}	10.43	10.37	11.04	10.96	10.71	10.66	11.07	10.35	11.45	12.35	15.5
MnO	0.17	0.17	0.18	0.18	0.16	0.19	0.16	0.13	0.18	0.15	0.21
MgO	7.73	7.88	7.15	7.14	7.72	7.78	7.36	8.11	9.02	5.11	5.03
CaO	10.89	10.91	10.52	10.52	11.23	11.15	11.18	11.08	10.88	10.48	9.9
Na_2O	2.66	2.68	2.87	2.83	2.86	2.7	2.16	1.71	1.96	1.06	–
K_2O	0.24	0.21	0.28	0.35	0.15	0.15	0.21	0.16	0.18	0.22	0.02
P_2O_5	0.13	0.12	0.18	0.19	0.1	0.13	0.11	0.17	0.1	0.16	0.39
LOI	1.1	1.18	1.03	1	0.98	1.08	1.85	1.68	1.07	3.57	3.7
Total	99.42	99.91	99.46	100.24	99.84	99.92	99.53	99.78	100.04	99.53	99.54
Mg#	63.3	63.9	60.1	60.3	62.7	63	60.8	64.6	64.7	49.1	43.1
Sc	38.3	37.7	40.9	42	42.1	41.2	40.4	34.63	44.11	25.53	33.81
V	227	219	261	253	262	237	215	219.4	279.5	300.7	307.5
Cr	343	356	285	395	346	365	283	232.5	316.2	59.55	38.57
Co	36.6	36.5	36.1	36.2	42.4	39.3	33.1	35.43	37.24	35.52	35.88
Ga	16.4	16.2	17.5	17.3	17.3	17.3	15.6	17.41	16.99	17.22	18.71
Rb	4.07	2.91	9.74	13.8	3.79	3.64	4.79	3.56	3.25	2.36	2.41
Sr	125	131	174	190	113	130	146	187.3	209.2	279.8	268.7
Y	26.7	26.3	30.3	31.1	28.2	28.1	27.2	27.23	28.19	25.31	33.21
Zr	41.7	36.5	66.2	62.8	58.5	64.1	59.6	49.1	45.2	44.5	36
Nb	2.45	2.44	3.36	3.55	2.08	2.49	2.12	3.76	3.71	4.03	4.18
Cs	2.31	2.3	6.01	7.9	1.11	1	2.41	2.43	3.16	2.58	2.5
Ba	45.9	34.5	25.9	56.4	12.5	46.9	57.8	27.5	22.4	7.8	6.2
Hf	1.48	1.23	2.06	2.03	2	2.01	1.33	1.79	1.87	1.55	1.35
Ta	0.26	0.24	0.36	0.27	0.16	0.19	0.18	0.34	0.28	0.33	0.31
Pb	2.16	1.78	2.05	2.32	2.08	2.06	2.06	2.11	1.89	1.41	1.16
Th	0.54	0.53	0.58	0.62	0.53	0.57	0.68	0.57	0.55	0.56	0.13
U	0.31	0.31	0.33	0.34	0.4	0.34	0.39	0.29	0.22	0.24	0.15

Table 3. (*Continued.*)

Sample No.	SN04-5	SN04-7	SN04-9	SN04-11	SN04-27	SN04-29	SN04-34	SN04-51	SN04-52	SN04-54	SN04-56
La	3.93	3.75	5.59	5.75	3.31	4.3	4.6	5.68	4.96	6.47	6.41
Ce	10.7	10.2	15.9	15.89	9.1	11.4	12.3	12.57	11.84	14.68	16.13
Pr	1.82	1.72	2.64	2.7	1.59	1.9	1.77	1.98	2.01	2.08	2.56
Nd	9.7	9.31	13.8	14.23	8.81	10.1	9.97	9.94	10.02	9.86	13.11
Sm	3.18	3.08	4.18	4.24	3.05	3.32	3.17	3.12	3.21	3.1	4.16
Eu	1.02	1.03	1.35	1.38	1.04	1.16	1.14	1.29	1.31	1.27	1.63
Gd	3.73	3.96	4.8	5.24	3.9	4.33	4.24	3.89	3.92	3.91	5.45
Tb	0.71	0.73	0.89	0.93	0.7	0.8	0.76	0.75	0.73	0.73	0.96
Dy	4.87	4.72	5.66	6	4.76	5.36	5.46	4.76	4.64	4.79	6.03
Ho	1.02	1.02	1.2	1.25	1.05	1.12	1.09	1.09	1.06	1.04	1.29
Er	2.83	2.93	3.3	3.47	2.95	3.17	3.33	2.92	2.91	2.8	3.32
Tm	0.43	0.44	0.48	0.51	0.42	0.46	0.47	0.45	0.47	0.42	0.48
Yb	2.71	2.64	2.3	3.07	2.67	2.86	2.32	2.72	2.75	2.77	3.03
Lu	0.41	0.39	0.44	0.45	0.4	0.41	0.45	0.42	0.4	0.42	0.45
La_N/Yb_N	1.04	1.02	1.34	1.34	0.89	1.08	1.42	1.38	1.19	1.54	1.4
Eu/Eu^*	0.91	0.9	0.92	0.89	0.92	0.94	0.95	1.14	1.14	1.13	1.06

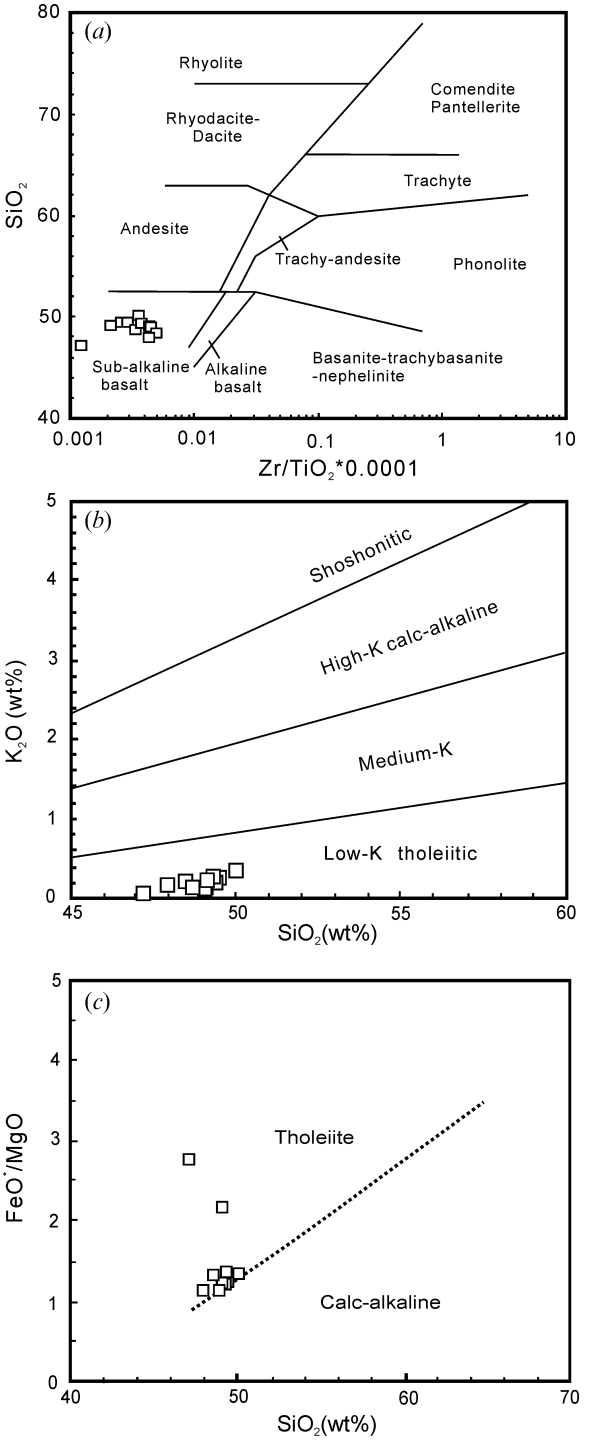

Figure 5. Plots (a) SiO_2 vs Zr/TiO_2 (Winchester and Floyd 1977), (b) K_2O vs SiO_2 (Ringwood 1989), and (c) FeO^*/MgO vs SiO_2 for the Sonidzuoqi hornblende gabbros.

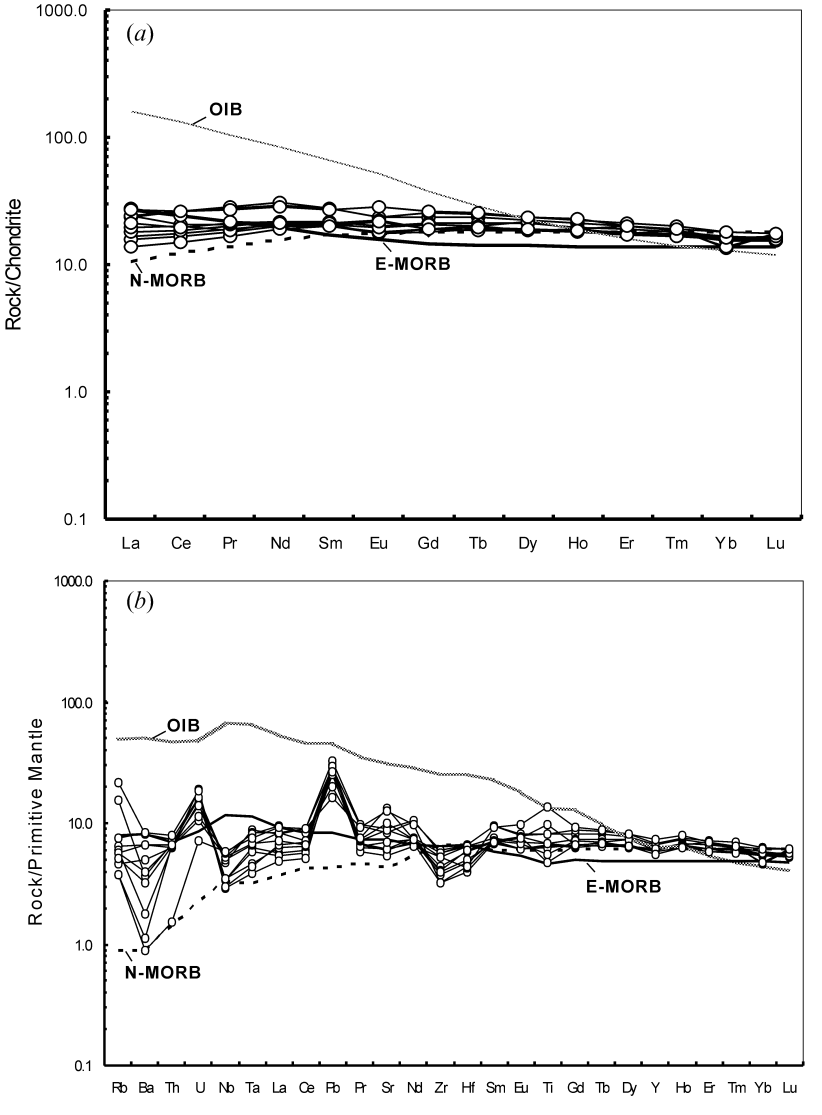

Figure 6. (a) Chondrite-normalized REE patterns and (b) primitive mantle-normalized trace element spidergrams for the Sonidzuowi hornblende gabbros. Normalization values are from Sun and McDonough (1989). Normal mid-ocean-ridge basalt (N-MORB), Enriched mid-ocean-ridge basalt (E-MORB) and ocean-island basalt (OIB) values are from Sun and McDonough (1989).

the large ion lithophile elements (e.g. Ba, Sr and Rb), whereas immobile elements include incompatible trace elements such as Ti, P, Zr, Nb, Ta, Hf, Th, Y, middle and heavy rare earth element (REE), as well as some transitional metals (e.g. Ni, Co, Cr, V). Therefore, emphasis will be placed on these in order to characterize the hornblende gabbros with respect to their original composition and possible tectonic environment of formation.

Most samples show high contents of MgO (Mg#=60 to 65), Cr (285–395 ppm) and V (219–262 ppm), and also exhibit an asthenospheric mantle-like isotopic composition [$^{87}Sr/^{86}Sr_{(t)} \approx 0.7030$ to 0.7042, $\varepsilon_{Nd}(t) \approx +4.35$ to $+7.80$;

Table 4. Rb–Sr and Sm–Nd isotopic compositions for Sonidzuoqi hornblende gabbros.

Sample No.	Rb (ppm)	Sr (ppm)	$^{87}Rb/^{86}Sr$	$^{87}Sr/^{86}Sr$	$\pm 2\acute{o}$	$(^{87}Sr/^{86}Sr)_t$	Sm	Nd	$^{147}Sm/^{144}Nd$	$^{143}Nd/^{144}Nd$	$\pm 2\acute{o}$	Initial Nd	e_{Nd} (t)	T_{DM} (Ma)	T_{DM2} (Ma)
SN04-5	4.095	139	0.0848	0.70379	12	0.70331	2.974	8.644	0.2083	0.513068	13	0.512522	7.8	2304	504
SN04-7	2.959	145.9	0.0585	0.70376	12	0.70343	3.007	8.724	0.2087	0.513036	12	0.512489	7.15	3447	553
SN04-9	10.42	189.7	0.158	0.70404	11	0.70314	4.079	12.9	0.1914	0.513012	13	0.512511	7.57	943	526
SN04-11	13.19	200.9	0.1886	0.70429	15	0.70322	3.901	12.49	0.1891	0.513011	14	0.512516	7.67	862	518
SN04-27	3.869	127.1	0.0886	0.70346	13	0.70296	3.125	8.353	0.2265	0.513106	11	0.512513	7.61	527	526
SN04-34	4.79	146	0.09448	0.70394	10	0.70338	3.17	9.97	0.1928	0.512018	15	0.512498	7.62	963	538
SN04-51	3.532	186.1	0.0547	0.70383	11	0.70352	3.113	9.874	0.1906	0.513008	12	0.512509	7.53	937	529
SN04-54	2.351	275.4	0.0246	0.70473	14	0.70416	2.891	8.852	0.1975	0.512863	12	0.512346	4.35	2685	783

Note: Chondrite uniform reservoir (CHUR) values ($^{87}Rb/^{86}Sr=0.0847$, $^{87}Sr/^{86}Sr=0.7045$, $^{147}Sm/^{144}Nd=0.1967$, $^{143}Nd/^{144}Nd=0.512638$) are used for the calculation. $\lambda_{Rb}=1.42\times10^{-11}$ year^{-1} (Steiger and Jäger 1977); $\lambda_{SM}=6.54\times10^{-12}$ year^{-1} (Lugmair and Harti 1978).

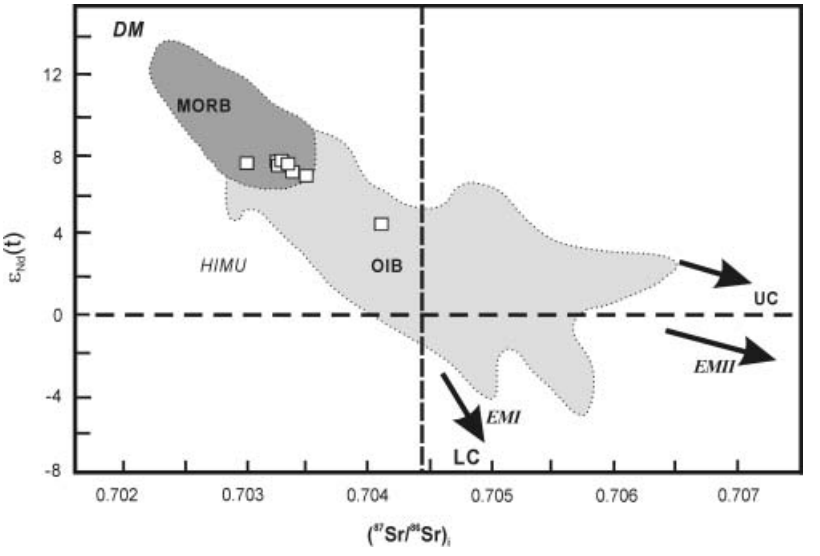

Figure 7. Plot of initial $\varepsilon_{Nd}(t)$ vs $(^{87}Sr/^{86}Sr)_i$ for the Sonidzuoqi hornblende gabbros (diagram after Zindler and Hart 1986). UC—upper crust; LC—lower crust; EMI and EMII—enriched mantle I and II sources; HIMU—high-μ mantle source; DM—depleted mantle source. MORB = mid-ocean ridge basalt; OIB = ocean island basalt.

$(^{206}Pb/^{204}Pb)_i \approx 17.46$ to 17.61] (Figures 7 and 8). This indicates that a component from a depleted MORB-like mantle was involved in their generation.

However, the samples display consistent depletion in HFSEs relative to fluid-mobile elements (e.g. negative Nb and Ta anomalies on the PM-normalized plot (Figure 6(b)). These characteristics are common in arc environments and generally attributed to subduction enrichment and fluid metasomatism in subduction zones (McCulloch and Gamble 1991; Pearce and Peate 1995).

Such dual source signatures are also evident on some tectonic discrimination diagrams. The samples have high Ti/V (20–50) and Ti/Zr typical of mid-ocean ridge basalts (Figure 9(a) and (b)), whereas the Th/Hf/Nb data are characteristic of island arcs (Figure 9(c)). On the Zr/Y vs Zr. diagram (Pearce and Norry 1979), samples plot in both the island-arc and ocean floor basalt fields (Figure 9(d)). The settings of both MORB and island arcs are commonly acknowledged to be unique to oceanic basins near convergent plate boundaries, where the influence of a marked subduction component signifies the geochemical characteristics of the mantle source (e.g. Taylor and Martinez 2003; Leat *et al.* 2004).

As demonstrated by Aldanmaz *et al.* (2008), the plot of Ta/Nd versus Th/Nb can be useful in characterizing the compositional effects of the subduction-related components and enriched versus depleted mantle sources on oceanic lavas (Figure 10). In the diagram, two distinct trends diverge strongly from NMORB compositions. The vertical trend, with increasing Ta/Nd ratios at near constant Th/Nb, could be the result of mixing between melts from MORB- and OIB-type sources, or alternatively, variable degrees of partial melting of a source similar in composition to the depleted MORB mantle; whereas the horizontal trend displays increase in the Th/Nb ratios with no significant change in Ta/Nd and can be interpreted to indicate MORB-subduction component mixing. This is specifically

Table 5. Pb isotopic compositions for Sonidzuoqi hornblende gabbros.

Sample No.	U	Th	Pb	$^{206}Pb/^{204}Pb$	$^{207}Pb/^{204}Pb$	$^{208}Pb/^{204}Pb$	$^{238}U/^{204}Pb$	$^{235}U/^{204}Pb$	$^{232}Th/^{204}Pb$	$(^{206}Pb/^{204}Pb)_i$	$(^{207}Pb/^{204}Pb)_i$	$(^{208}Pb/^{204}Pb)_i$	Δ7/4	Δ8/4
SN04-5	0.31	0.54	2.16	18.252	15.578	38.248	9.07	0.07	16.32	17.642	15.544	37.905	14.1	95
SN04-7	0.31	0.53	1.78	18.284	15.593	38.299	11.02	0.08	19.46	17.542	15.552	37.89	15.95	105.5
SN04-9	0.33	0.58	2.05	18.291	15.55	38.152	10.16	0.07	18.45	17.607	15.512	37.765	11.26	85.1
SN04-11	0.34	0.62	2.32	18.24	15.548	38.104	9.24	0.07	17.41	17.618	15.514	37.739	11.29	81.1
SN04-27	0.4	0.53	2.08	18.28	15.548	38.176	12.14	0.09	16.62	17.463	15.503	37.827	11.89	108.7
SN04-34	0.39	0.68	2.06	18.313	15.561	38.209	11.96	0.09	21.54	17.508	15.517	37.757	12.77	96.3
SN04-51	0.29	0.57	2.11	18.265	15.572	38.273	8.69	0.06	17.34	17.68	15.54	37.903	13.22	90

Note: $\lambda_{u238}=1.55125\times10^{-10}$ year^{-1}; $\lambda_{u235}=9.8485\times10^{-10}$ year^{-1}; $\lambda_{Th232}=4.9475\times10^{-11}$ year^{-1} (Steiger and Jäger 1977). $\Delta7/4=[(^{207}Pb/^{204}Pb)_I-(^{207}Pb/^{204}Pb)_{NHRL}]\times100$; $\Delta8/4=[(^{208}Pb/^{204}Pb)_i-(^{208}Pb/^{204}Pb)_{NHRL}]\times100$; $(^{207}Pb/^{204}Pb)_{NHRL}=0.1084\times(^{206}Pb/^{204}Pb)_i+13.491$ (Hart 1984); $(^{208}Pb/^{204}Pb)_{NHRL}=1.209\times(^{206}Pb/^{204}Pb)_i+15.627$ (Hart 1984).

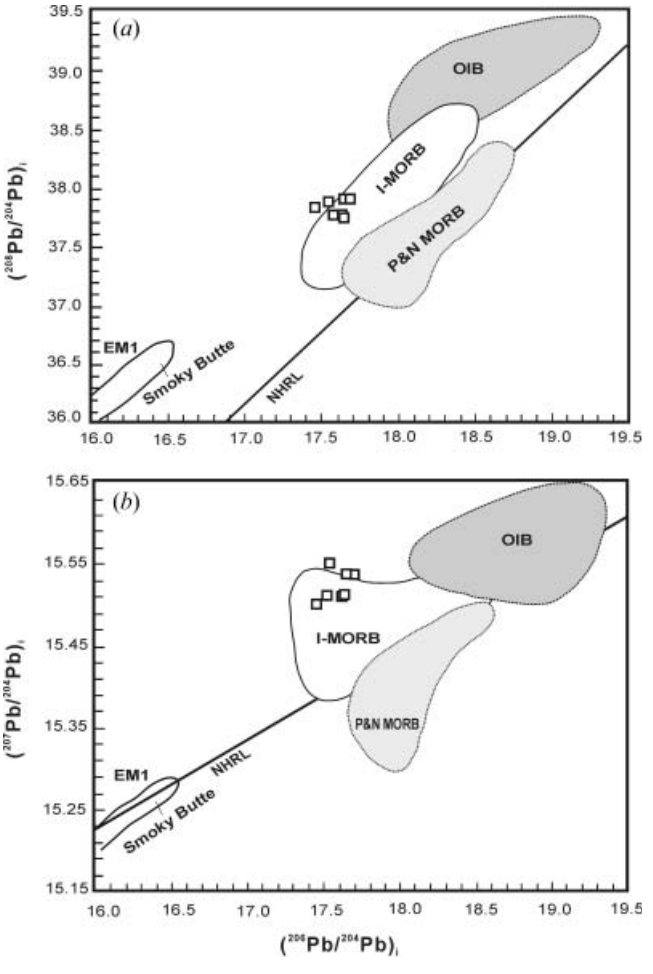

Figure 8. (a) Initial $^{208}Pb/^{204}Pb$ and (b) $^{207}Pb/^{204}Pb$ vs. $^{206}Pb/^{204}Pb$ for the Sonidzuoqi hornblende gabbros. Fields for I-MORB (Indian MORB), P&NMORB (Pacific and North Atlantic MORB), OIB and NHRL (northern hemisphere reference line) are taken from Zindler and Hart (1986) and Barry and Kent (1998); and the Smoky Butte lamprophyres from Fraser *et al.* (1985). MORB = mid-oceanic ridge basalt; OIB = oceanic island basalt; EMI = enriched mantle I.

true in this case: the distribution of the samples along the horizontal trend suggests mixing between MORB and island arc tholeiite (IAT) (Figure 10).

Subduction components

The nature of the source region from which the melts were generated can be deduced from ratio-ratio plots that have a more incompatible element divided by a less incompatible element, such as the Th/Yb versus Nb/Yb plot (Pearce *et al.* 1995). Since the denominator is incompatible, partial melting of a source region lowers the value of both ratios and produces the source depletion vector (Figure 11(a)); while liquid and cumulate fractionation trends exhibit vectors parallel but opposite in direction to the source depletion one (Snow *et al.* 2007). Moreover, addition of a subduction-derived fluid should increase the Th/Yb ratio without significantly affecting the Nb/Yb ratio, owing to negligible Nb in subduction fluids (Pearce *et al.*

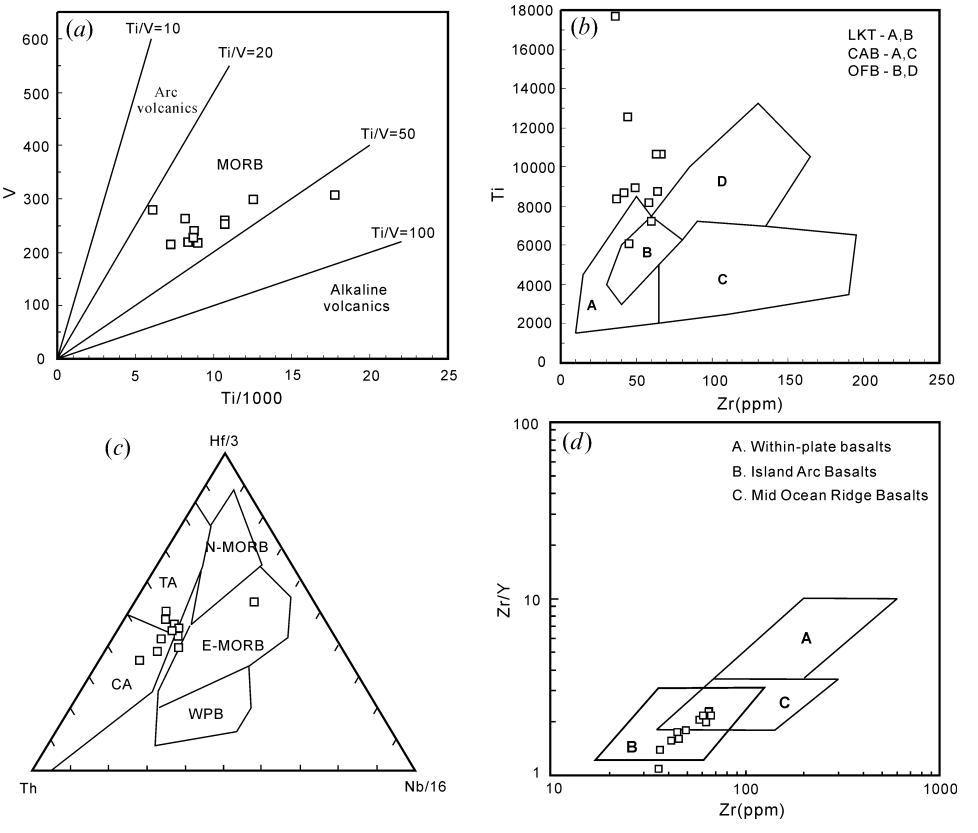

Figure 9. Plots (a) V vs Ti/1000 (Shervais 1982), (b) Ti vs Zr (Pearce and Cann 1973), (c) Hf/3-Th-Nb/16 (Wood 1980) and (d) Zr vs Zr/Y (Pearce and Norry 1979) for the Sonidzuoqi hornblende gabbros. In (a), MORB = mid-oceanic ridge basalt; in (b), LKT = low-K tholeiite, CAB = calc-alkali basalt, OFB = ocean floor basalt; in (c), CA = calc-alkaline basalt, TA = island-arc tholeiite, N-MORB = normal mid-ocean-ridge basalt, E-MORB = enriched mid-ocean-ridge basalt, WPB = within-plate basalt.

1995). This results in the subduction component vector. Therefore, by extrapolating along the vectors, it is possible to gauge the level of source depletion for various melts. Data from the Sonidzuoqi gabbros suggest that there was a significant subduction component involved in their formation and that liquid fractionation was a significant process.

In general, siliceous melts and aqueous fluids constitute two significant contributions in creating subduction components in SSZ mantle melting regions. Their relative importance can be further examined using Hf–Nd systematics. With their similar incompatibilities, HFSE and REE are generally expected to behave coherently in mantle melting systems where relatively homogenized mantle domains melt to produce MORB and OIB magmas. In areas of plate convergence and subduction, however, relative enrichment in REE results in negative anomalies in Hf concentrations with respect to Nd (e.g. Thirlwall *et al.* 1994; Pearce and Peate 1995). In this respect, a log–log binary plot of Hf/Yb vs Nd/Yb can be very instructive (Figure 11(b); Pearce *et al.* 1999). On this plot, these element ratios exhibit a straight-line relationship and form a horizontal mantle trend if the basaltic melt is produced by partial melting of ambient mantle compositions (e.g. MORB–OIB

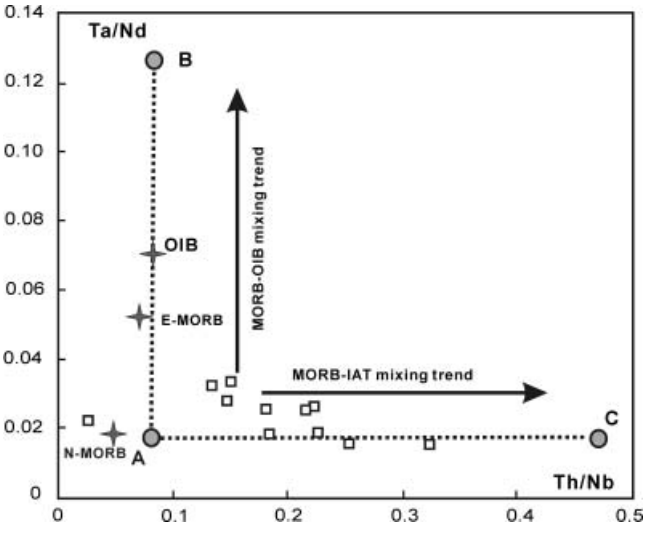

Figure 10. Variation of Ta/Nd vs Th/Nb for the Sonidzuoqi hornblende gabbros. Two mixing trends and end-member components shown in the figure are as represented and discussed by Aldanmaz *et al.* (2008), with A defined by 17% melting of a depleted mantle source, B defined by 4% melting of an enriched mantle source and C defined by 20% melting of a subduction-enriched mantle source.

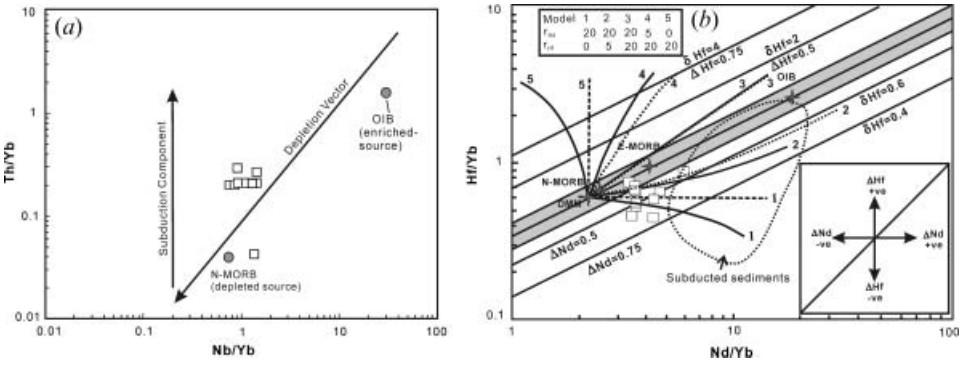

Figure 11. (a) Th/Yb vs Nb/Yb diagram for the Sonidzuoqi hornblende gabbros (after Pearce *et al.* 1995). Normal mid-ocean-ridge basalt (N-MORB) and ocean-island basalt (OIB) values are from Sun and McDonough (1989). (b) Hf/Yb vs Nd/Yb co-variations (after Pearce *et al.* 1999) for the Sonidzuoqi hornblende gabbros. ΔHf and ΔNd define extent of positive and negative displacements of samples from the mantle array (shown as shaded area) defined by average MORB–OIB compositions (Pearce *et al.* 1999). Δ values indicate displacements from the mantle array and positive Δ value corresponds to high element ratios with respect to the mantle array. Equal Hf anomalies (δ Hf) are represented by straight lines parallel to the MORB–OIB array, with positive ΔNd values corresponding to negative Hf anomalies. Positive ΔNd values record the proportion of subducted Nd in mantle sources. δHf describes the negative Hf anomaly as a Hf depletion, whereas ΔNd describes the anomaly as a Nd enrichment. Both ΔHf and ΔNd can be expressed in terms of the element compositions of the mantle and subduction zone end-members. Mixing trends between depleted MORB mantle (DMM) and subducted pelagic sediment are also shown for a mass fraction of subduction component in the mantle between 0.05 and 0.2 and a range of values of r_{Nd} and r_{Hf} at r_{Yb} equal to 0 (dashed lines) or 2 (solid lines). Representative ratios (r) for Hf and Nd between the subduction component and the mantle are shown in the inset.

production). Displacements from the mantle trend, however, should be associated with addition of components having Nd/Hf ratios different from the ambient mantle-derived melt compositions. As shown in Figure 11(b), most of the Sonidzuoqi gabbro samples are displaced from the 'mantle array' defined by MORB–OIB compositions toward lower Hf/Yb, consistent with their slight to moderate negative Hf anomalies ($\delta Hf < 1$). Hafnium anomalies shown by these samples seem to be consistent with the addition of a subduction-related component, in which the Nd/Hf ratio exceeds a value of about 20. It is suggested that Hf, although soluble to varying degrees in siliceous melts, has a low solubility in aqueous fluids derived from subducted materials and is unlikely to have been transported to the mantle in fluids originating from slab dehydration (e.g. Barry *et al.* 2006). In contrast, Nd is more soluble in both subduction-derived fluids and melts. Thus, elevated Nd/Hf ratios in slab-derived fluxes would be inconsistent with melting of sediment or oceanic crust, but could only be explained if aqueous fluids dominated subduction-related inputs to the basalt source region (Pearce *et al.* 1999). Therefore, our data suggest that the Sonidzuoqi gabbros are the products of melting of depleted MORB mantle that presumably interacted with subduction fluid originating largely from slab dehydration.

REE modelling

To quantitatively evaluate the possible mantle sources and melting conditions required to generate melts similar to those analysed in this study, we adopted the standard non-modal batch melting equations of Shaw (1970) to model the REE patterns of the gabbros with K_D values from Gorring and Kay (2001). Modelling parameters, mantle source composition, melt and source modes, and the degree of partial melting are listed in Table 6. The source modal composition is $Ol_{0.60}Opx_{0.28}Cpx_{0.11}Sp_{0.01}$, while concentrations of REE in the peridotitic source are assumed to be 1.3 times primitive mantle of Sun and McDonough (1989) with the exception of La and Ce. With their relatively high Mg# (60.1–64.7) and Cr (>250 ppm) abundances, most of our samples are considered to approximate to the primary melt (or minimally modified melt).

The results of the partial melting modelling for REE are presented in Figure 12. It shows that 10–19% partial melting of the possible mantle source successfully reproduces the chondrite-normalized REE patterns of the less differentiated gabbroic samples.

Tectonic implications

As outlined by Shervais (2001), the processes of crust generation and tectonic evolution during life cycles of SSZ ophiolites can be recorded by the temporal geochemical changes of magmatic events that took place over the entire history of the relevant ocean basins. This is especially the case for the widely scattered ophiolitic units at Sonidzuoqi, which directly document semi-continuous phases of the tectono-magmatic evolution of the Palaeo-Asian oceanic basin in terms of mantle source and melt generation.

Being the southernmost and oldest magmatic unit of the early to middle Palaeozoic Sonidzuoqi orogen, the ophiolitic mélange provides evidence of MORB-OIB geochemical signatures and thus likely represents an oceanic crustal portion generated during the birth stage of a SSZ ophiolite. Specifically, the mantle peridotites are rich in Mg and Ni, and poor in Al and Ca (Zhang and Wu 1999),

Table 6. Model parameters and results of non-modal batch partial melting calculations (ppm).

Phase	Source mode				Phase	Melt mode				
Olivine	0.60				Olivine	0.25				
OPX	0.28				OPX	0.25				
CPX	0.11				CPX	0.3				
Spinel	0.01				Spinel	0.2				
	Partial melting degree			Source		Partition coefficients				
REE	10%	15%	19%	S	Ol	Opx	Cpx	Sp	Grt	
La	6.580	4.473	3.561	0.687	0.000007	0.0005	0.0536	0.0006	0.01	
Ce	16.574	11.394	9.114	1.775	0.00001	0.0009	0.0858	0.0006	0.021	
Nd	15.004	10.708	8.712	1.76	0.00007	0.009	0.1873	0.0006	0.087	
Sm	4.482	3.314	2.743	0.58	0.0007	0.02	0.291	0.0006	0.217	
Eu	1.624	1.219	1.016	0.22	0.00095	0.03	0.3288	0.0006	0.4	
Gd	5.525	4.206	3.531	0.77	0.0012	0.04	0.367	0.0006	0.6	
Dy	6.264	4.901	4.174	0.96	0.004	0.06	0.442	0.0015	1.3	
Ho	1.389	1.086	0.925	0.21	0.0065	0.065	0.4145	0.0023	2	
Er	4.053	3.165	2.693	0.62	0.009	0.07	0.387	0.003	3	
Yb	3.703	2.980	2.578	0.64	0.023	0.1	0.43	0.0045	4.03	
Lu	0.499	0.411	0.360	0.10	0.035	0.15	0.433	0.0045	4.03	

Note: Sources: S – 1.3 times primitive mantle of Sun and McDonough (1989) with the exception of La and Ce, which are equal to those of Sun and McDonough (1989); Source and melt mineralogy are taken arbitrarily, but similar to those used in other partial melting calculations (McKenzie and O'Nions 1995; Tang *et al.* 2006).

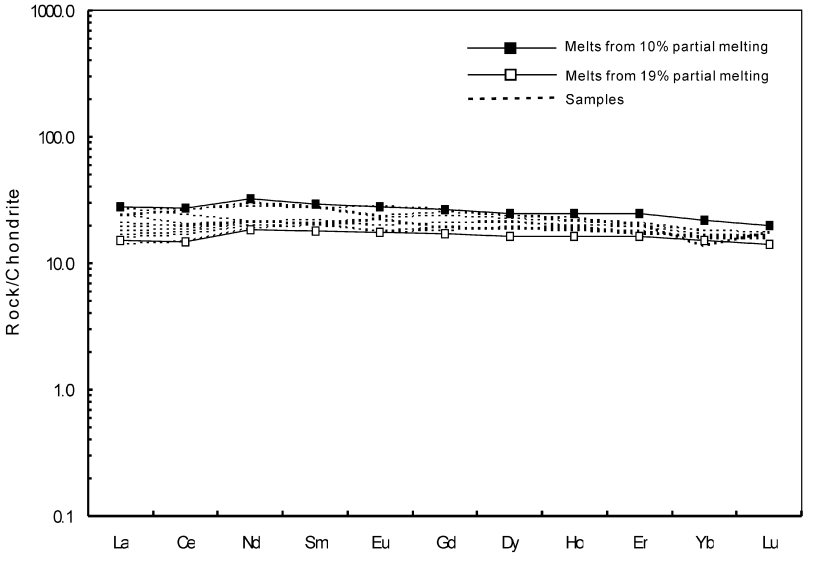

Figure 12. Chondrite-normalized REE patterns for the determined values and the non-modal batch melting model results for the Sonidzuoqi hornblende gabbros.

indicating that they are highly depleted mantle residues. The MORB-type tholeiites exhibit low-Ti geochemical affinity (Zhang and Wu 1999, Huang *et al.* 2006), while the OIB-type basalts display high-Ti geochemical affinity (Huang *et al.* 2006). The magmatic processes during this stage are rather similar to those observed in presently active oceanic spreading systems (e.g. the East Pacific Rise: Niu *et al.* 2002), where melt production is characterized by multi-component mantle interaction and mixing of melts from variably enriched and depleted mantle domains and where crust production is dominated by along-axis pressure-release melting of depleted MORB mantle with some contribution from off-axis melting of more enriched sub-lithospheric sources (Aldanmaz *et al.* 2008).

Subsequent evolution from MORB to island arc magmatism is recorded by the Shadui intrusive rocks with ages of 483 to 471 Ma. These intrusions, ranging in rock type from cumulate gabbro, quartz diorite and tonalite, are characterized by low-Ti and -K affinity, LILE enrichment and HFSE depletion (Jian *et al.* 2008). It is suggested that they formed from partial melting of sub-arc mantle with subsequent fractionation (Jian *et al.* 2008), and thus represented a typical juvenile middle-lower arc crustal portion generated during the youth and maturity stages of the SSZ ophiolite.

Other typical plutonic rocks formed during these stages are represented by the Baiyanbaolido TTG pluton with ages of 498 to 461 Ma (Chen *et al.* 2000; Shi *et al.* 2005a). Their distinctive geochemical characteristics (Chen *et al.* 2000; Shi *et al.* 2005a), such as intermediate affinity between adakites and normal arc rocks, lower $\varepsilon_{Nd}(t)$ values and more radiogenic $^{87}Sr/^{86}Sr$ ratios than classic intra-oceanic arcs (e.g. the Aleutians), argue for a petrogenetic scenario of ridge-trench interaction. Under this scenario, trench sediments melted due to anomalously elevated thermal gradients and contributed to near-trench melts and arc magmas. Concomitantly, considerable slab melt/upper mantle interaction occurred and triggered subsequent melting of the upper mantle.

The hornblende gabbros described herein, with their occurrence in the northern part of the magmatic belt, compatible age record and MORB-IAT geochemical

affinity, signify that an intervening active spreading centre finally entered the trench and subduction zone. The dual geochemical signatures shown by the magmatism during this stage are consistent with two-stage melting processes required for producing oceanic basin basalts near convergent plate boundaries (e.g. McCulloch and Gamble 1991; Pearce *et al*. 2005). During these processes, the initial stage of melt extraction depletes the source in all incompatible trace elements (e.g. LILE and HFSE), leaving a depleted and refractory mantle residue; while subsequent melting occurs after or during an influx of aqueous fluids carrying the subduction-related enriched components and triggers a second-stage melting event in the SSZ residual mantle that had previously yielded MORB-type melts at the spreading centre. This indicates that the SSZ ophiolite came to its 'death stage' and also marks the turning point that transformed oceanic lithosphere to continental crust.

Ridge-ophiolite collision indicative of the death of the SSZ ophiolite is also witnessed by coeval high-K, calc-alkaline granites with ages of ca. 425 Ma (Shi *et al.* 2005b). Their transitional trace element affinity between volcanic arc granite and syn-collisional granite, together with their hybrid isotopic signatures of depleted mantle and continental material, leads to a petrogenetic scenario consistent with slab break-off or delamination (Atherton and Ghani 2002).

As such, the tectono-magmatic development during the early to middle Palaeozoic Sonidzuoqi orogen provides a Palaeo-Asian case study for testing the consistency of the life cycles of SSZs as advocated by Shervais (2001). The progressive evolution in geochemical affinity from MORB-OIB, through IAV, to MORB/ IAT as recorded by the discrete units of the Sonidzuoqi ophiolite, attests to multi-staged crustal generation during a protracted geodynamic history, involving seafloor spreading, proto-arc rifting and ridge collision, analogous to many presently-active arc-basin systems.

Conclusions

Hornblende K–Ar and SHRIMP zircon U–Pb dating, petrologic examination and geochemical study on a suite of hornblende gabbros document an episode of Late Silurian MORB-IAT magmatism at Sonidzuoqi in Inner Mongolia. Their distinctive hydrous petrologic character and MORB-IAT geochemical affinity argue for a hydrous basaltic parental magma that is consistent with the coupling between MORB-type mantle upwelling and fluid influx from slab devolatilization. Such a petrogenetic scenario signifies that an intervening active spreading centre finally entered the trench and a SSZ ophiolite came to the final 'death' stage. These unique hornblende gabbros, together with the pre-500 Ma ophiolitic mélange with MORB-OIB geochemical affinity, the 483–471 Ma intrusive arc rocks, the 498–461 Ma TTG plutons and the 427–423 Ma calc-alkaline granites, document systematic multi-staged crustal generation during the protracted life cycle of a SSZ ophiolite.

Acknowledgements

This study was financially supported by the Major State Basic Research Programme of the People's Republic of China (Grant No. 2006CB403504), the Knowledge Innovation Programme of the Chinese Academy of Sciences (Grant No. KZCX2-YW-103) and the National Natural Science Foundation of China (Grant No. 40534022 and 40873026). The authors thank Mr H. Li and Ms X. D. Jin for major- and trace-element analysis, and Dr C.F. Li and Ms Xiu-Li Wang for assistance with Sr–Nd–Pb isotope analyses. This is The Institute for Geoscience Research (TIGeR) publication No. 168.

References

Aldanmaz, E., Yaliniz, M.K., Güctekin, A., and Göncüoğlu, M.C., 2008, Geochemical characteristics of mafic lavas from the Neotethyan ophiolites in western Turkey: implications for heterogeneous source contribution during variable stages of ocean crust generation: Geological Magazine, v. 145, p. 37–54.

Arculus, R.J., and Wills, K.J.A., 1980, The petrology of plutonic blocks and inclusions from the Lesser Antilles island arc: Journal of Petrology, v. 21, p. 743–799.

Atherton, M.P., and Ghani, A.A., 2002, Slab breakoff: A model for Caledonian, Late Granite syn-collisional magmatism in the orthotectonic (metamorphic) zone of Scotland and Donegal, Ireland: Lithos, v. 62, p. 65–85.

Barry, T.L., and Kent, R.W., 1998, Cenozoic magmatism in Mongolia and the origin of central and east Asian basalts., *in* Flower, M.F.J., Chung, S.L., Lo, C.H., and Lee, T.Y., eds., Mantle Dynamics and Plate Interactions in East Asia: Washinton, DC, American Geophysical Union, p. 347–364.

Barry, T.L., Pearce, J.A., Leat, P.T., Millar, I.L., and le Roex, A.P., 2006, Hf isotope evidence for selective mobility of high-field-strength elements in a subduction setting: South Sandwich Islands: Earth and Planetary Science Letters, v. 252, p. 223–244.

Bedard, J.H., 1999, Petrogenesis of boninites from the Betts Cove ophiolite, Newfoundland, Canada: Identification of subducted source components: Journal of Petrology, v. 40, p. 1853–1889.

Burns, L.E., 1985, The Border Ranges ultramafic and mafic complex, south-central Alaska: Cumulate fractionates of island-arc volcanics: Canadian Journal of Earth Science, v. 22, p. 1020–1038.

Chen, B., Jahn, B.M., Wilde, S., and Xu, B., 2000, Two contrasting Paleozoic magmatic belts in northern Inner Mongolia, China: Petrogenesis and tectonic implications: Tectonophysics, v. 328, p. 157–182.

Coish, R.A., Hickey, R., and Frey, F.A., 1982, Rare earth element geochemistry of the Betts Cve ophiolite, Newfoundland: Complexities in ophiolite formation: Geochimica et Cosmochim Acta, v. 46, p. 2117–2134.

Davis, G.A., Zheng, Y., Wang, C., Darby, B.J., Zhang, C., and Gehrels, G.E., 2001, Mesozoic tectonic evolution of the Yanshan fold and thrust belt, with emphasis on Hebei and Liaoning provinces, northern China, *in* Hendrix, M.S., and Davis, G.A., eds., Paleozoic and Mesozoic Tectonic Evolution of Central and Eastern Asia: From Continental Assembly to Intracontinental Deformation, Geological Society of America Memoir 194, p. 171–197.

Fan, W.M., Guo, F., Wang, Y.J., and Lin, G., 2003, Late Mesozoic calcalkaline volcanism of post-orogenic extension in the northern Da Hinggan Mountains, northeastern China: Journal of Volcanology and Geotherm Research, v. 121, p. 115–135.

Fraser, K.J., Hawkesworth, C.J., Erland, A.J., Mitchell, R.H., and Scottsmith, B.H., 1985, Sr–Nd–Pb isotopic and minor element geochemistry of lamprophyres and kimberlites: Earth and Planetary Science Letters, v. 76, p. 57–70.

Gorring, M.L., and Kay, S.M., 2001, Mantle processes and sources of Neogene slab window magmas from southern Patagonia, Argentina: Journal of Petrology, v. 42, p. 1067–1094.

Hart, S.R., 1984, A large-scale isotope anomaly in the southern hemisphere mantle: Nature, v. 309, p. 753–757.

Hong, D.W., Huang, H.Z., Xiao, Y.J., Xu, H.M., and Jin, M.Y., 1995, Permian alkaline granites in central Inner Mongolia and their geodynamic significance: Acta Geologica Sinica, v. 8, p. 27–39.

Hu, X., Xu, C., and Niu, S., 1990, Evolution of the Early Paleozoic Continental Margin in Northern Margin of the North China Platform: Beijing, Beijing University Press, p. 6–23 (in Chinese with English abstract).

Huang, J., Zhao, Z., Zhang, H., Hou, Y., Chen, Y., Zhang, B., and Depaolo, D.J., 2006, Elemental and Sr–Nd–Pb isotopic geochemistry of the Wenduermiao and Bayanaobao-Jiaoqier ophiolites, Inner Mongolia: Constraints for the characteristics of

the mantle domain of eastern Palaeo-Asian Ocean: Acta Petrologica Sinica, v. 22, p. 2889–2900.

Inner Monglian Bureau of Geology and Mineral Resources (IMBGMR), 1998, 1: 50000 scale regional geological maps of Sonidzuoqi, Zulegetu, Changtuximusumu, Shaertala and Bayannuoersumu.

Jian, P., Liu, D.Y., Kroner, A., Windley, B.F., Shi, Y.R., Zhang, F.Q., Shi, G.H., Miao, L.C., Zhang, W., Zhang, Q., Zhang, L., and Ren, J., 2008, Time scale of an early to mid-Paleozoic orogenic cycle of the long-lived Central Asian Orogenic belt, Inner Mongolia of China: Implications for continental growth: Lithos, v. 101, p. 233–259.

Johannes, W., 1978, Melting of plagioclase in the system Ab–An–H_2O and Qz–Ab–An–H_2O at P_{H2O}=5 kbars an equilibrium problem: Contributions to Mineralogy and Petrology, v. 66, p. 295–303.

Khain, E.V., Bibikova, E.V., Kröner, A., Zhuravlev, D.Z., Sklyarov, E.V., Fedotova, A.A., and Kravchenko-Berezhnoy, I.R., 2002, The most ancient ophiolite of the Central Asian fold belt: U–Pb and Pb–Pb zircon ages for the Dunzhugur Complex, Eastern Sayan, Siberia, and geodynamic implications: Earth and Planetary Science Letters, v. 199, p. 311–325.

Khain, E.V., Bibikova, E.V., Salnikova, E.B., Kröner, A., Gibsher, A.S., Didenko, A.N., Degtyarev, K.E., and Fedotova, A.A., 2003, The Paleo-Asian ocean in the Neoproterozoic and early Paleozoic: New geochronologic data and paleotectonic reconstructions: Precambrian Research, v. 122, p. 329–358.

Kocak, K., Isik, F., Arslan, M., and Zedef, V., 2005, Petrological and source region characteristics of ophiolitic hornblende gabbros from the Aksaray and Kayseri regions, central Anatolian crystalline complex, Turkey: Journal of Asian Earth Sciences, v. 25, p. 883–891.

Kuzmichev, A., Kröner, A., Hegner, E., Dunyi, L., and Yusheng, W., 2005, The Shishkhid ophiolite, northern Mongolia: A key to the reconstruction of a Neoproterozoic island-arc system in central Asia: Precambrian Research, v. 138, p. 125–150.

Leake, B.E., Woolley, A.R., Arps, C.E.S., Birch, W.D., Gilbert, M.C., Grice, J.D., Hawthorne, F.C., Kato, A., Kisch, H.J., Krivovichev, V.G., Linthout, K., Laird, J., Mandarino, J.A., Maresch, W.V., Nickel, E.H., Rock, N.M.S., Schumacher, J.C., Smith, D.C., Stephenson, N.C.N., Ungaretti, L., Whittaker, E.J.W., and Youzhi, G., 1997, Nomenclature of amphiboles: Report of the subcomittee on amphiboles of the international mineralogical association, Commission on new minerals and mineral names: American Mineralogist, v. 82, p. 1019–1037.

Leat, P.T., Pearce, J.A., Barker, P.F., Millar, I.L., Barry, T.L., and Larter, R.D., 2004, Magma genesis and mantle flow at a subducting slab edge: The South Sandwich arc-basin system: Earth and Planetary Science Letters, v. 227, p. 17–35.

Liu, D.Y., Jian, P., Zhang, Q., Zhang, F.Q., Shi, Y.R., Shi, G.H., Zhang, N.Q., and Tao, H., 2003, SHRIMP dating of adakites in the Tulinkai ophiolite, Inner Mongolia: Evidence for the early Paleozoic subduction: Acta Geologica Sinica, v. 77, p. 318–327.

Liu, W., Siebel, W., Li, X., and Pan, X., 2005, Petrogenesis of the Linxi granitoids, northern Inner Mongolia of China: Constraints on basaltic underplating: Chemical Geology, v. 219, p. 3–35.

Ludwig, K., 2001, User manual for isoplot/EX (2.49). Berkeley Geochronology Centre Special Publication No. 1a. 55 p.

Lugmair, G.W., and Harti, K., 1978, Lunar initial $^{143}Nd/^{144}Nd$: Differential evolution of the lunar crust and mantle: Earth and Planetary Science Letters, v. 39, p. 349–357.

McCulloch, M.T., and Gamble, J.A., 1991, Geochemical and geodynamical constraints on subduction zone magmatism: Earth and Planetary Science Letters, v. 102, p. 358–374.

McKenzie, D., and O'Nions, R.K., 1995, The source regions of oceanic island basalts: Journal of Petrology, v. 36, p. 133–159.

Miao, L., Zhang, F., Fan, W., and Liu, D., 2007, Phanerozoic evolution of the Inner Mongolia-Daxinganling orogenic belt in North China: Constraints from geochronology of ophiolites and associated formations, *in* Zhai, M.G., Windley, B.F., Kusky, T.M.,

and Meng, Q.R., eds., Mesozoic Sub-Continental Lithospheric Thinning Under Eastern Asia: Geological Society London Special Publications 280, p. 223–237.

Niu, Y., Regelous, M., Wendt, I.J., Batiza, R., and O'Hara, M.J., 2002, Geochemistry of near-EPR seamounts: Importance of source vs. process and the origin of enriched mantle component: Earth and Planetary Science Letters, v. 199, p. 327–341.

Nozaka, T., and Liu, Y., 2002, Petrology of the Hegenshan ophiolite and its implications for the tectonic evolution of northern China: Earth and Planetary Science Letters, v. 202, p. 89–104.

Pearce, J.A., 2003, Supra-subduction zone ophiolites: The search for modern analogues, *in* Dilek, Y., and Newcomb, S., eds., Ophiolite Concept and the Evolution of Geological Thought: Geological Society of America Special Paper, v. 373, p. 269–293.

———, 2005, Mantle preconditioning by melt extraction during flow: Theory and petrogenetic implications: Journal of Petrology, v. 46, p. 973–997.

Pearce, J.A., Baker, P.E., Harvey, P.K., and Luff., L.W., 1995, Geochemical evidence for subduction fluxes, mentle melting and fractional crystallization beneath the south Sandwich island arc: Journal of Petrology, v. 36, p. 1073–1104.

Pearce, J.A., and Cann, J.R., 1973, Tectonic setting of basic volcanic rocks determined using trace element analyses: Earth and Planetary Science Letters, v. 19, p. 290–300.

Pearce, J.A., Kempton, P.D., Nowell, G.M., and Noble, S.R., 1999, Hf–Nd element and isotope perspective on the nature and provenance of mantle and subduction components in Western Pacific arc-basin systems: Journal of Petrology, v. 40, p. 1579–1611.

Pearce, J.A., and Norry, M.J., 1979, Petrogenetic implications of Ti, Zr, Y and Nb variations in volcanic rocks: Contributions to Mineralogy and Petrology, v. 69, p. 33–47.

Pearce, J.A., and Peate, D.W., 1995, Tectonic implications of the composition of volcanic arc magmas: Annual Reviews of Earth and Planetary Science, v. 23, p. 251–285.

Ringwood, P.C., 1989, Boundary lines within petrologic diagrams which use oxides of major and minor elements: Lithos, v. 22, p. 247–263.

Sengör, A.M.C., and Natal'in, B.A., 1996, Paleotectonics of Asia: fragments of a synthesis, *in* Yin, A., and Harrison, T.M., eds., The Tectonic Evolution of Asia: Cambridge, Cambridge University Press, p. 486–641.

Sengör, A.M.C., Natal'in, B.A., and Burtman, V.S., 1993, Evolution of the Altaid tectonic collage and Palaeozoic crustal growth in Eurasia: Nature, v. 364, p. 299–307.

Shao, J.A., 1991, Crust Evolution in the Middle Part of the Northern Margin of Sino-Korean Plate: Beijing, Peking University press.

Shaw, D.M., 1970, Trace element fractionation during anatexis: Geochim et Cosmochim Acta, v. 34, p. 237–243.

Shervais, J.W., 1982, Ti-V plots and the petrogenesis of modern and ophiolitic lavas: Earth and Planetary Science Letters, v. 59, p. 101–118.

———, 2001, Birth, death, and resurrection: The life cycle of suprasubduction zone ophiolites: Geochemistry, Geophysics, Geosystems, v. 2, doi:10.1029/2000GC000080.

Shervais, J.W., Kimbrough, D.L., Renne, P., Murchey, B., Snow, C.A., Schaman, R.M.Z., and Beaman, J., 2004, Multi-stage origin of the Coast Range ophiolite, California: Implication for the life cycle of supra-subduction zone ophiolites: International Geology Review, v. 46, p. 289–315.

Shi, G.H., Liu, D.Y., Zhang, F.Q., Jian, P., Miao, L.C., Shi, Y.R., and Tao, H., 2003, SHRIMP U–Pb zircon geochronology and its implications on the Xilin Gol Complex, Inner Mongolia, China: Chinese Science Bulletin, v. 48, p. 2742–2748.

Shi, G.H., Miao, L.C., Zhang, F.Q., Jian, P., Fan, W.M., and Liu, D.Y., 2004, The age and its regional tectonic implications of the Xilinhaote A-type granites, Inner Mongolia: Chinese Science Bulletin, v. 49, p. 384–389.

Shi, Y.R., Liu, D.Y., Zhang, Q., Jian, P., Zhang, F.Q., Miao, L.C., Shi, G.H., Zhang, L.Q., and Tao, H., 2005a, The petrogenesis and SHRIMP dating of the Baiyinbaolidao

adakitic rocks in southern Sonidzuoqi, Inner Mongolia: Acta Petrologica Sinica, v. 21, p. 143–150.

Shi, Y.R., Liu, D.Y., Jian, P., Zhang, Q., Zhang, F.Q., Miao, L.C., Shi, G.H., Zhang, L.Q., and Tao, H., 2005b, Zircon SHRIMP dating of Krich granites in Sonid Zuoqi: Geological Bulletin of China, v. 21, p. 424–428 (in Chinese with English abstract).

Shong, H.S., Tao, J.X., Bao, Y.W., and Hao, X.Y., 2003, The arc-basin system and tectonic significance of early Paleozoic in Baiyunebo area, Inner Mongolia: Geological Survey and Research, v. 26, p. 160–168 (in Chinese with English abstract).

Sisson, T.W., and Grove, T.L., 1993, Temperatures and H_2O contents of low-MgO high-alumina basalts: Contributions to Mineralogy and Petrology, v. 113, p. 166–184.

Snow, C.A., 2007, Petrotectonic evolution and melt modeling of the Penon Blanco arc, central Sierra Nevada foothills, California: Geological Society of America Bulletin, v. 119, p. 1014–1024.

Steiger, R.H., and Jäger, E., 1977, Subcommission on geochronology: Convention on the use of decay constants in geochronology and cosmochronology: Earth and Planetary Science Letters, v. 36, p. 359–362.

Sun, S.S., and McDonough, W.F., 1989, Chemical and isotopic systematics of oceanic basalts: implications for mantle composition and processes, *in* Saunders, A.D., and Norry, M.J., eds., Magmatism in the Ocean Basins: Geological Society of London Special Publication 42, p. 528–548.

Tang, K.D., 1990, Tectonic development of Paleozoic foldbelts at the northern margin of the Sino-Korean craton: Tectonics, v. 9, p. 249–260.

Tang, Y.J., Zhang, H.F., and Ying, J.F., 2006, Asthenosphere-lithospheric mantle interaction in an extensional regime: implication from the geochemistry of Cenozoic basalts from Taihang Mountains, North China craton: Chemical Geology, v. 233, p. 309–327.

Tao, J.X., Xu, L.Q., He, F., and Su, M.T., 2005, Petrological evidence for subduction of the early Paleozoic oceanic crust in the Bater Obo, Inner Mongolia: Geological Survey and Research, v. 28, p. 1–8 (in Chinese with English abstract).

Taylor, B., and Martinez, F., 2003, Back-arc basin basalt systematics: Earth and Planetary Science Letters, v. 210, p. 481–497.

Thirlwall, M.F., Smith, T.E., Graham, A.M., Theodorou, N., Hollings, P., Davidson, J.P., and Arculus, R.J., 1994, High field strength element anomalies in arc lavas: Source or process?: Journal of Petrology, v. 35, p. 819–838.

Wang, Q., Liu, X., and Li, J., 1991, Plate tectonics between Cathaysia and Angaraland in China: Beijing, Peking University Press, 151 p.

Winchester, J.A., and Floyd, P.A., 1977, Geochemical discrimination of different magma series and their differentiation products using immobile elements: Chemical Geology, v. 20, p. 325–342.

Windley, B.F., Alexeiev, D., Xiao, W.J., Kroner, A., and Badarch, G., 2007, Tectonic models for accretion of the Central Asian Orogenic belt: Journal of the Geological Society, London, v. 164, p. 31–47.

Wood, D.A., 1980, The application of a Th–Hf–Ta diagram to problems of tectonomagmatic classification and to establishing the nature of crustal contamination of basaltic lavas of the British Tertiary volcanic province: Earth and Planetary Science Letters, v. 50, p. 11–30.

Wu, F.Y., Sun, D.Y., Li, H.M., Jahn, B.M., and Wilde, S.A., 2002, A-type granites in northeastern China: Age and geochemical constraints on their petrogenesis: Chemical Geology, v. 187, p. 143–173.

Xiao, W., Windley, B.F., Hao, J., and Zhai, M., 2003, Accretion leading to collision and the Permian Solonker suture, Inner Mongolia, China: Termination of the central Asian orogenic belt: Tectonics, v. 22, p. 1484–1505.

Xu, B., Charvet, J., and Zhang, F.Q., 2001, Primary study on petrology and geochronology of the blueschist in Sunitezuoqi, northern Inner Mongolia: Chinese Journal of Geology, v. 36, p. 424–434 (in Chinese with English abstract).

Xu, B., and Chen, B., 1997, Framework and evolution of the middle Paleozoic orogenic belt between Siberian and North China plate in northern Inner Mongolia: Science in China (Series D), v. 40, p. 463–469.

Yin, A., and Nie, S., 1996, A Phanerozoic palinspastic reconstruction of China and its neighboring regions, *in* Yin, A., and Harrison, T.M., eds., Tectonic Evolution of Asia: Cambridge, Cambridge University Press, p. 442–485.

Zhang, C., and Wu, T., 1999, Features and tectonic implications of the ophiolitic melange in the southern Sonidzuoqi, Inner Mongolia: Acta Geologica Sinica, v. 34, p. 381–389.

Zhang, X.H., Zhang, H.F., Tang, Y.J., Wilde, S.A., and Hu, Z.C., 2008, Geochemistry of Permian bimodal volcanic rocks from Central Inner Mongolia, North China: Implication for tectonic setting and phanerozoic continental growth in Central Asian Orogenic Belt: Chemical Geology, v. 249, p. 261–281.

Zhu, Y.F., Sun, S.H., Mao, Q., and Zhao, G., 2004, Geochemistry of the Xilingele complex, Inner Mongolia: A historic record from Rodinia accretion to continental collision after closure of the Paleo-Asian ocean: Geological Journal of China University, v. 10, p. 343–355.

Zindler, A., and Hart, S.R., 1986, Chemical geodynamics: Annual Review of Earth and Planetary Sciences, v. 14, p. 493–571.